Int. J. Electrochem. Sci., 12 **(2017)** 2412 – 2428, doi: 10.20964/2017.03.75

International Journal of
ELECTROCHEMICAL
SCIENCE
www.electrochemsci.org

Galvanic Corrosion Behavior of 907A/ Titanium Couple in Simulated Seawater

Xiaodong Zhang[1], *Xiaoqing Du*[2,*], *Chao Cai*[3], *Zhao Zhang*[2,*]

[1] MIUR, Naval University of Engineering, Wuhan 430033, China
[2] Department of Chemistry, Zhejiang University, Hangzhou 310027, China
[3] Department of Chemistry, Ningxia University, Yinchuan750021, China
[*]E-mail: eaglezzy@zju.edu.cn, amyzju88@163.com

Received: 3 January 2017 / *Accepted:* 29 January 2017 / *Published:* 12 February 2017

The corrosion behaviors of 907A and 907A/ titanium galvanic couple (GC) in seawater have been studied by using electrochemical impedance spectroscopy and electrochemical noise techniques in conjunction with scanning electron microscope method. The results show that, both the corrosion process of 907A and 907A /Ti GC can be divided into two stages but with different demarcation point, and the potential difference between Ti and 907A not only markedly accelerates the corrosion process of 907A in 907A/Ti GC, but also possibly changes its corrosion mechanism. The electrochemical active energy E_a derived from the corrosion noise has been first adopted to characterize the corrosion process of 907A and 907A/Ti GC in seawater, and it is found that the larger the E_a value, the higher the corrosion rate.

Keywords: 907A/Ti; Galvanic corrosion; Electrochemical noise; Electrochemical impedance spectroscopy;

1. INTRODUCTION

Ship-built steel 907A is a kind of low alloy steels with high strength [1], which is independently developed in China, and has been widely used in ship manufacture and other coastal facilities [2]. However, up to now, only a few of domestic researches have been conducted on the relationship between the mechanical behavior of 907A and its constitutes [2, 3]or microstructures [4], the cathodic polarization on its susceptibility to hydrogen embrittlement [1]and the protective effect of some inhibitors on its galvanic corrosion with ZL102 Al alloy [5].

Generally, the mechanical properties of low alloy steels are significantly degraded by corrosion because of their reduction in cross-section and their increasing surface roughness [6], therefore, as a

kind of low alloy steels, the corrosion process of 907A should also damage its function as a component of facilities, especially, the main servicing environment for 907A is the ocean with high content of different aggressive particles. Moreover, in order to meet some special demands from the industrial products design [5, 7], 907A has to be coupled with other metals, especially titanium (Ti) and copper (Cu), the galvanic corrosion caused by the mutual electron transfer (through the combination) between the two coupled partners is inevitable [8], which also undoubtedly accelerate the corrosion process of 907A and markedly degrade its properties. Therefore, the study of the corrosion behaviors for 907A and its galvanic couple with Ti in seawater is of important significance.

Nowadays, weight-loss [9], potentiodynamic polarization [3] and zero resistance ammeter (ZRA) [10, 11] have been widely adopted to determine the galvanic corrosion parameters, such as the galvanic corrosion potential and current. However, the so-called electrochemical noise (EN) technique [12], which acts as a non-destructive testing technology and can provide more information about the corrosion process, is rarely reported in the studies of galvanic corrosion.

Therefore, this paper aims to monitor the corrosion process of 907A and its electric couple with Ti in simulated seawater by using EN and electrochemical impedance spectroscopy (EIS) techniques, especially to elucidate the influence of Ti on the corrosion behavior of its coupled 907A.

2. EXPERIMENTAL

2.1. Material and specimen preparation

The rod specimens of 0.40 cm in diameter have been cut from 907A plate. Then the specimens were connected respectively to a copper wire at one end, sealed using nylon with the other end exposed as the working surface. Before experiments, the working surface was polished by abrasive papers through 500–1200 grade and velvet, washed by twice distilled water, and finally degreased with acetone.

907A/Ti galvanic couple was prepared by embedding 907A column into the titanium cylinder with inner and outer diameters of 0.40 cm and 0.56 cm, then the couple was encapsulated using nylon, the exposed area of each metal was equal to 0.13 cm^2.

2.2. Measurement methods

EIS tests were recorded with an impedance measurement apparatus (PARSTAT 2273, Advanced Electrochemical System) at the rest potential, the applied sinusoidal voltage amplitude was 5 mV and the sweep always initiated from the frequency of 100 kHz to 0.01 Hz. The tests were performed at different immersion times in a conventional three-electrode compartment cell. The rod 907A or the coupled 907A/Ti specimen prepared in section 2.1 was the working electrode, a large platinum foil was used as auxiliary electrode and a saturated calomel electrode (SCE) was employed as the reference.

EN was monitored as a function of time between the working electrode and SCE using a Powerlab/4s apparatus (e-DAQ), which was controlled by Chart4 software using the Windows XP operating system. This equipment allows resolutions of 1 μV for voltage signals and 1 pA for current signals. EN data of 4096 points was collected at 4 points/s each time, which conditions define a frequency window in which most usual corrosion processes can be detected. The analytical results for maximum entropy method (MEM) technique and fast wavelet transform (FWT) were obtained by specific data technique. All tests were carried out in artificial seawater (pH 7.5) whose main components were listed in our previous study [8] and at room temperature (25 ± 2) ºC. During the above experiments, the corrosion morphologies of the samples were observed at different immersion time using a JEOL USA JSM-5510LV scanning electron microscope (SEM) with a field emission gun operated at 3 kV.

3. RESULTS AND DISCUSSION

3.1. Corrosion behavior of 907A

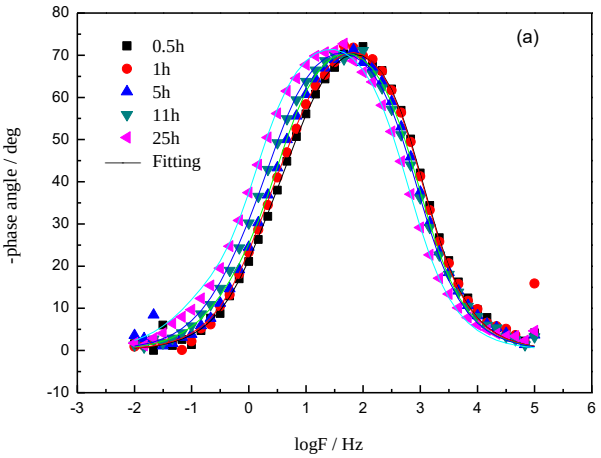

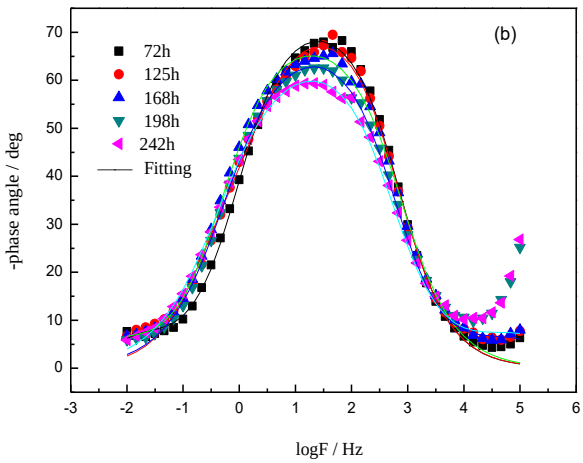

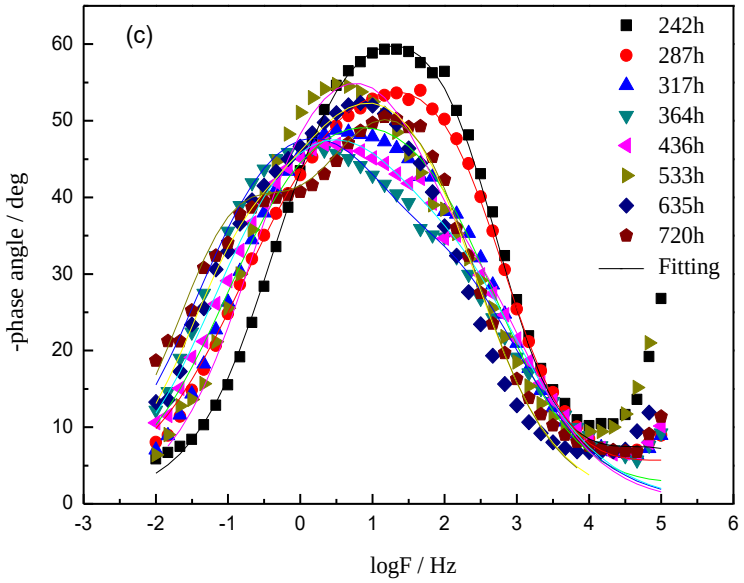

Figure 1. EIS plots of 907A corrosion at different times, (a-b) 0-242h, (c) 248-720h.

In order to elucidate the galvanic corrosion behavior of the coupled 907A/Ti in seawater, the corrosion behavior of 907A has been first investigated using EIS and EN techniques. Fig. 1 shows the typical EIS evolution features of 907A corrosion in seawater. With the help of both the features of the EIS diagrams and the method developed by Wit [13, 14] simultaneously, it can be determined that, in the first 242 h (Fig. 1a-b), there is only one time constant in the EIS plots. Whilst, from 242 h to 720 h(Fig. 1c), the EIS plots become wide and flat or directly show two peaks at 1Hz and 0.1Hz, which means that with the increase of corrosion time, two time constants are needed to fit the EIS plots. The reason is that more and more corrosion products accumulated on the matrix surface, which leads to a new double electrode layer and displays as another time constant.

The equivalent electrical circuits (EECs) shown in Fig.2 have been adopted to fit the EIS plots by using Z-view software and the fitted results are listed in Tables 1-2.

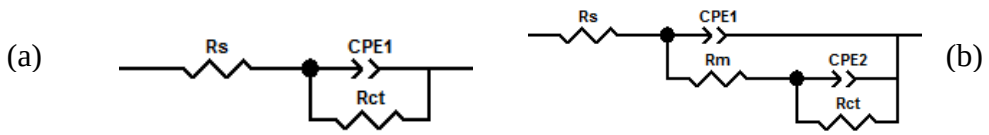

Figure 2. EEC used for simulating the impedance spectra of 907A corroding in seawater (a)R_S is the solution resistance, CPE1 is the double layer capacitance, *R*ct is charge transfer resistance. (b)R_S is the solution resistance, CPE1 is the capacitance of outer passivating film and corrosion product layer, *R*m is the membrane resistance of outer passivating film and corrosion products, CPE2 is the double layer capacitance, *R*ct is charge transfer resistance.

Table 1. Analyzed EIS results for 907A corrosion in seawater from 0.5h to 242h

Time/ h	R_S/Ω	CPE1-P/μF	n1	Rct/Ω
0.5	22.8	17.184	0.85641	4156
1.0	23.07	19.992	0.85936	4698
2.5	23.23	20.148	0.86348	5904
3.5	23.36	21.306	0.86141	4721
6.0	23.64	22.406	0.85621	5010
11	23.28	23.236	0.84919	5875
12	23.56	26.379	0.84948	6144
25	26.71	27.017	0.85316	7687
29	26.67	30.201	0.84359	7937
52	38.17	30.768	0.83424	10233
72	40.71	26.518	0.82332	11223
96	45.05	23.668	0.81173	12510
101	44.54	22.543	0.81844	12174
120	48.40	21.879	0.80088	14666
149	50.01	24.067	0.77482	12833
168	48.66	27.137	0.78620	16076
173	47.98	26.469	0.78378	14514
198	55.03	27.152	0.76765	13599
219	57.51	29.509	0.76241	15000
242	59.73	30.727	0.73394	13703
248	58.69	36.445	0.69375	14263

Table 2. Analyzed EIS results for 907A corrosion in seawater from 263h to 720h

Time/ h	Rs/Ω	CPE1-P/μF	n1	Rm/Ω	CPE2-P/μF	n2	Rct/Ω
263	62.58	40.421	0.71858	13713	977.83	0.82704	3536
287	62.69	49.407	0.69308	8678	117.61	0.82704	6706
317	64.07	95.656	0.63497	3094	17.646	0.82704	8297
336	64.83	114.66	0.61907	1919	41.813	0.82704	11857
364	72.62	123.69	0.59058	2406	27.841	0.82704	15133
388	76.06	113.85	0.58783	2590	20.288	0.82704	15818
407	81.12	101.45	0.59520	4527	15.437	0.82704	14066
436	88.36	88.492	0.59618	2835	11.658	0.82704	14602
455	97.10	49.690	0.6448	1038	87.318	0.82704	15132
484	99.20	36.992	0.68745	877.7	10.272	0.82704	15687
503	100.9	36.657	0.69137	842.7	10.387	0.82704	15719
533	91.05	40.195	0.68767	722.6	10.529	0.82704	14123
575	92.84	54.205	0.66756	1027	5.3192	0.82704	15333
599	92.98	65.680	0.65446	1660	2.2994	0.82704	15255
635	100.3	64.973	0.68360	10941	147.42	0.82704	10018
681	92.41	68.837	0.68337	7463	135.09	0.82704	13021
707	88.81	76.350	0.66965	5667	142.64	0.82704	10727
727	84.81	70.281	0.69298	4986	156.85	0.82704	13198

Capacitance has a relationship with the corroding area as following:

$$C \propto \frac{\varepsilon S}{d} \quad (1)$$

where C is the capacitance, S is the surface area, ε is dielectric constant and d is the thickness. The ongoing corrosion process will gradually enlarge the interface between the electrode and the aggressive solutions, and the ε of a metal is somewhat lower than that of its oxide, both of them consequently result in the increase of CPE1-P. The influence of corrosion process on S can be partially verified by the corroding morphologies of 907A (Fig.3).

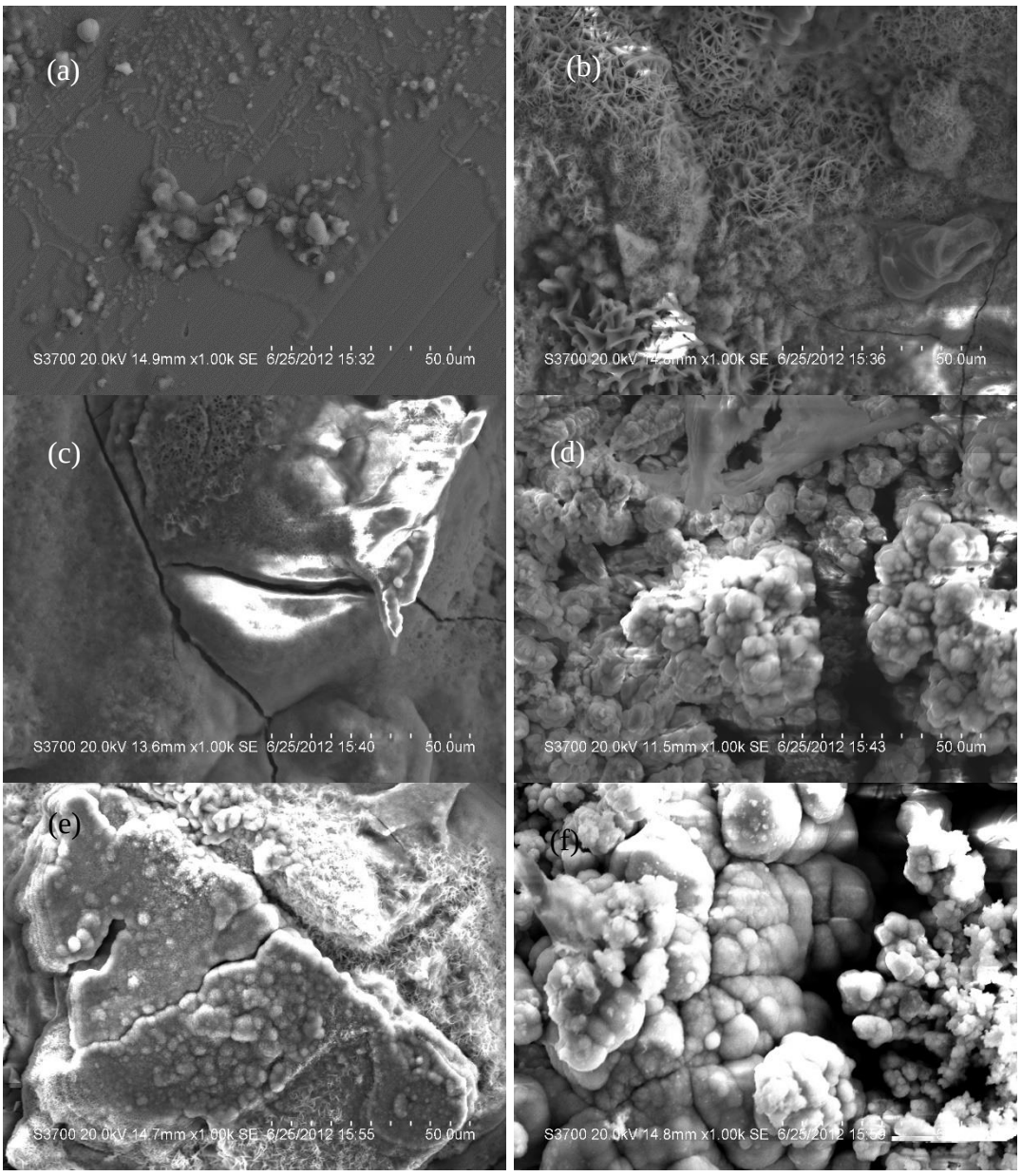

Figure 3. SEM morphologies of the 907A corrosion at different times, (a) 0.5 h; (b) 24 h; (c) 120 h;(d) 240 h;(e) 480 h;(f) 720 h.

Fig.3a indicates that the metal matrix surface is relatively smooth with only a small amount of corrosion products at 0.5h, which results in a small value of CPE1-P. However, when extending the

immersion time, many meshy (Fig.3b), nubbly (Fig.3c) or cauliflower shaped (Fig.3d-f) corrosion products are generated, which leads to both the increase and variation of the corroding area *S* and so does the value of CPE1-P (Tables 1-2).It should be mentioned that, the CPE1-P in Fig. 2b expresses as the mixed capacitance of the outer passivating film and corrosion product layer.

Generally, the reciprocal of the sum of *R*ct and *R*m (Fig. 2) is widely used to characterize the corrosion rate [15], the larger the sum of *R*ct and *R*m, the lower the corrosion rate. Fig. 4 clearly shows the corrosion rate of 907A decreases with the corrosion time.

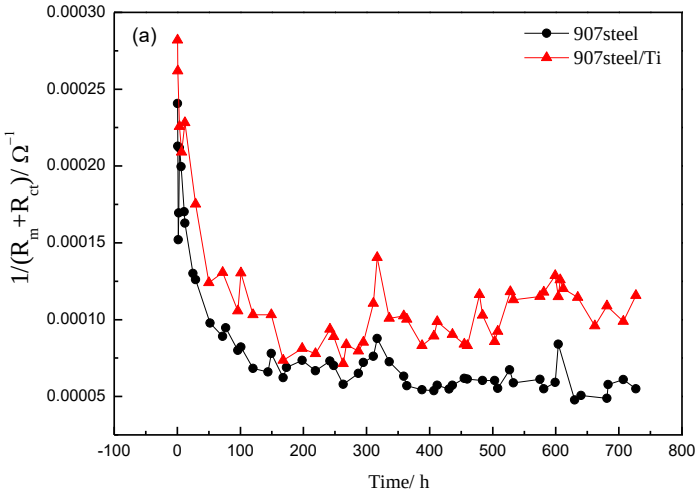

Figure 4. The dependence of the corrosion rate of 907A and 907A/Ti GC with immersion time

For the reason that the main component of 907A is Fe, when immersing 907A in seawater, the following reactions 2-6 will happen [16-19],

anode： $Fe \rightarrow Fe^{2+} + 2e^{-}$ (2)

cathode: $\frac{1}{2}O_2 + H_2O + 2e^{-} \rightarrow 2OH^{-}$ (3)

$Fe^{2+} + 2OH^{-} \rightarrow Fe(OH)_2$ (4)

$4Fe(OH)_2 + O_2 + 2H_2O \rightarrow 4Fe(OH)_3$ (5)

$Fe + Cl^{-} \Leftrightarrow (FeCl^{-})_{ads}$ (6)

As the corrosion continues, more and more corrosion products will accumulate on the matrix surface, which will block the transmission path of O_2 or Cl^- from corrosive medium to metal surfaces (Reactions 5-6). On the other hand, based on the nature that the corrosion product $Fe(OH)_3$ (reactions 5) are always porous and unconsolidated, and possesses poor adhesion with matrix [19], the accumulated corrosion products on the matrix surface will crack or even leave off from the matrix due to the limited space of the matrix surface(Fig.3e), which therefore momently increases the corrosion area (*S*) and decreases *R*ct, and subsequently enhances the corrosion rate [20]. Therefore, the formation, accumulation and the cracking or even separation of corrosion products will simultaneously change the area of the corroding surface, the resistances of passivating film and charge transfer, and subsequently causes the fluctuations on both CPE1-P (Table 2) and the corrosion rate (Fig.4).

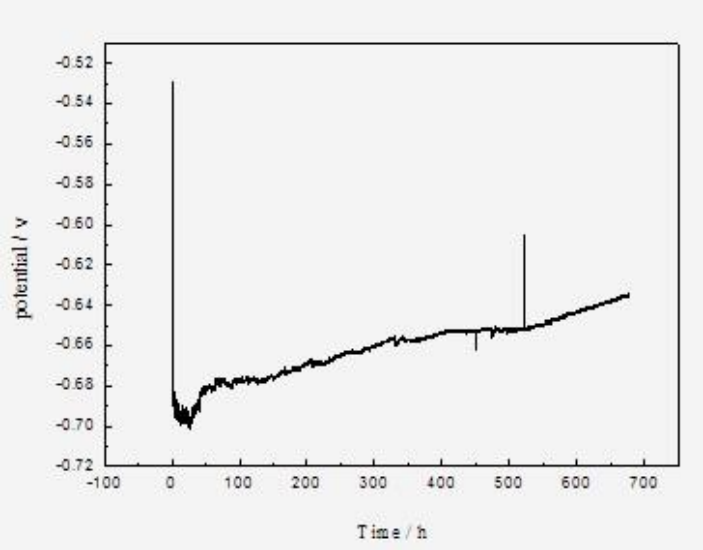

Figure 5. The electrochemical potential noise of 907A corroding in seawater for 700 hours

Fig. 5 is the potential noise (without elimination of dc drift) of 907A corroding in seawater for 700 h. The ensemble potential noise plot can be divided into two segments, i.e., the initial short time with the corrosion potential jump negatively, the second segment with the corrosion potential drift positively. The first potential decrease is due to the direct contact between the initial nude 907A matrix and the corrosive particles Cl^- and O_2, which reduces the corrosion active points and also results in the fast increase of *R*ct as elucidated above (Table 1). With further extension of immersion time, the generation and accumulation of corrosion products (Fig. 3), especially the formation, gradual completion and thickening of the inner corrosion products layer, will slowly cut down the direct exposure of nude matrix 907A, and therefore drifts the electrode potential positively (Fig. 5).

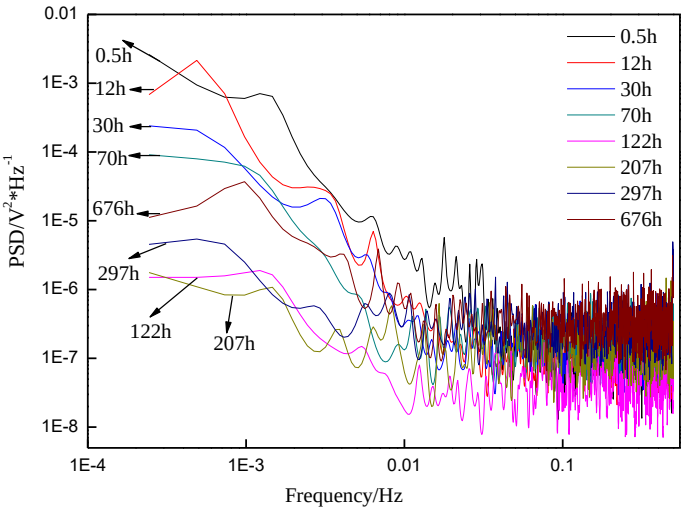

Figure 6. The PSD plots of 907A corrosion in seawater at different times

Whilst, the synergetic effects from the generation/accumulation, cracking (Fig. 3c), exfoliation (Fig. 3e), and stripping of the corrosion products, and also the crevice corrosion (which usually presents as the potential jump due to the simultaneous formation of vast pits) will result in the potential fluctuation.

The potential noise shown in Fig. 5 has been analyzed using MEM technique [21] according to its different corrosion stages, the obtained spectral power density plots (PSD) are shown in Fig. 6. Then, the white noise level (W), the cut-off frequency (f_c) and the high frequency linear slope (k) of PSD are obtained using mathematical methods [22-24] and adopted to calculate the corrosion indexes S_E and S_G [8]:

$$S_E = f_c^{\,2}\sqrt{k} \tag{7}$$

$$S_G = \frac{W}{f_c k} \tag{8}$$

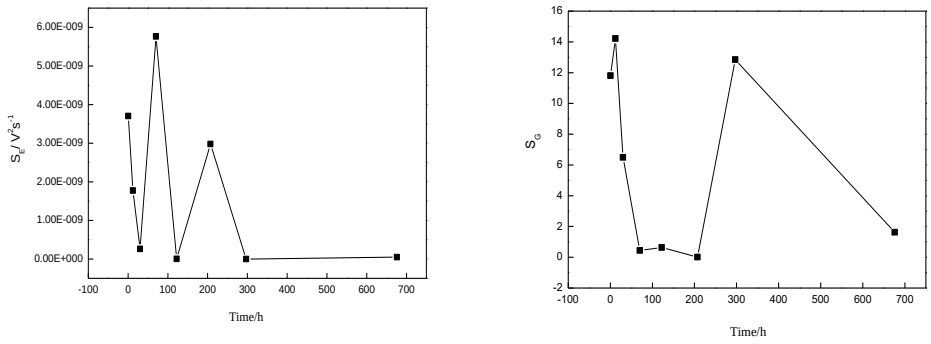

Figure 7. The S_E and S_G value of 907A corrosion in seawater at different times

Fig. 7 shows the evolution features of S_E and S_G with time. A complete corrosion process should simultaneously contain fast and slow reaction steps. As the value of S_E is only determined by k and f_c, which are the characteristic parameters of fast reaction steps, S_E is used to describe the fast steps (or the reactions of smaller time constant), such as the metastable and stable pitting corrosion or crystal nucleation. So, S_G mainly reflects the characteristics of slow steps (or the reactions of larger time constant) such as the diffusion and migration of particles, growth of pits or crystal nucleus, crevice corrosion and so on [25]. According to Fig. 7, the whole investigated corrosion process of 907A can also be divided into two stages. In the first stage (from the onset of the corrosion to ca. 200 h), because there exist many surface defects or imperfections such as plateau edges, kinks, vacancies and emergent screw dislocations [26, 27], the initial corrosion mainly occurs at the already existed surface defects and the aggressive particles (eg. O_2 and Cl^-) have to migrate to thus sites to initiate corrosion, which consumes the aggressive particles adjacent to these defects and results in their local concentration gradient. Therefore, both the initial pitting corrosion and the migration of the aggressive particles are rapid, which certainly brings about both the large initial values of S_E and S_G (Fig. 7); Whilst, because the inner corrosion products layer formed in the above initial pitting corrosion process is relatively defective or not compact (the initial pitting corrosion mainly takes place on the surface defects of 907A), and especially due to the autocatalytic corrosion effect of the discrete occluded pitting pores

[28], the influence of the aggressive particles migrating from bulk solution to pits' tip on corrosion process reduces gradually, therefore, in this stage, S_E shows large fluctuations and S_G decreases(Fig. 7).

With the prolongation of corrosion time (the second stage), much corrosion products are generated and accumulated on 907A surface (Fig. 3), especially its inner compact layer is almost formed, and the main corrosion type changes from the pitting corrosion of smaller time constant to the intergranular or exfoliation corrosion of larger time constant (pitting mainly occurs along the grain boundary, and their corrosion products bring about tensile stress) [29], which not only consumes most aggressive particles adjacent to the interface of 907A/corrosion products, forms large concentration gradient of the aggressive particles and presents as the large fluctuations of S_G, but also results in the small value of S_E (Fig. 7).

Compare Fig. 7 with Fig. 5, it can also be found that the demarcation point to distinguish the two corrosion stages is much different, which is caused by the fact that the data in Fig. 5 simultaneously contain both the dc drift and the EN signals in the real sense, and both of them are overlapped. Whereas, when performing MEM analysis of the data in Fig. 5, the dc drift is eliminated in advance by using polynomial fitting method. In other words, the demarcation point of the two corrosion stages obtained by Fig. 7 is much more correct, which can also be verified by its comparison with the demarcation point (ca. 240 h) obtained in EIS analyses (Fig. 1 and Fig. 4).

The time domain EN data in Fig. 5 are also analyzed using FWT method [30-33], the obtained results are shown in Fig. 8, where the electrochemical active energy (E_a) is defined as the sum of the energy deposited in crystals d_1 to d_6[12, 28],

$$E_a = E_{d1} + E_{d2} + E_{d3} + E_{d4} + E_{d5} + E_{d6} \quad (9)$$

In equation (9), d_j is named crystal *j*, which is obtained by the FWT analysis of EN data using db4 wavelets [25,29,34,35], E_{dj} is the energy deposited in crystal *j*, $E_{d1}+E_{d2}+E_{d3}$ and $E_{d4}+E_{d5}+E_{d6}$ are the energies of pits' nucleation and their growth processes respectively [12,28].

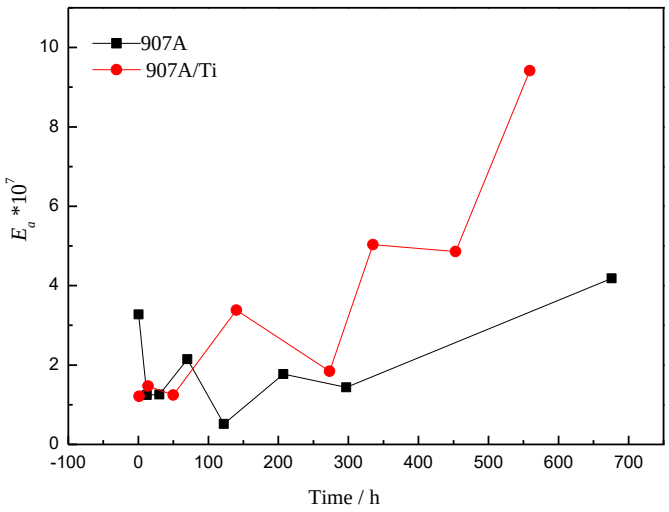

Figure 9. The relationship of E_a with corrosion time for 907A and 907A/Ti GC corroding in artificial seawater

From Fig. 9, it can be seen that E_a shows the same variation tendency as that of S_E (Fig. 7) except that the rising rate of the former is larger than that of the latter after corrosion for 300 h. The reason is that the information provided by S_E mainly reflects the characteristics of the fast steps (or the reactions of smaller time constant), such as the metastable and stable pitting corrosion or crystal nucleation [41], whereas E_a simultaneously reflects the characteristics of pitting (smaller time constant), pits' growth and other type corrosion processes (larger time constant) [12, 25, 28].

3.2 Corrosion behavior of 907A/Ti galvanic couple (GC)

Fig.10 shows the typical EIS plots of 907A/Ti GC in seawater. By using the same methods elucidated in Section 3.1, the whole corrosion process of 907A/Ti GC can also be divided into two stages, ie., the first stage from 0h to ca. 168h and the second stage for the remainder time. Therefore, the EIS plots in Fig.10 are also fitted using the same EECs shown in Fig.2, and the analyzed results are listed in Table 3-4.

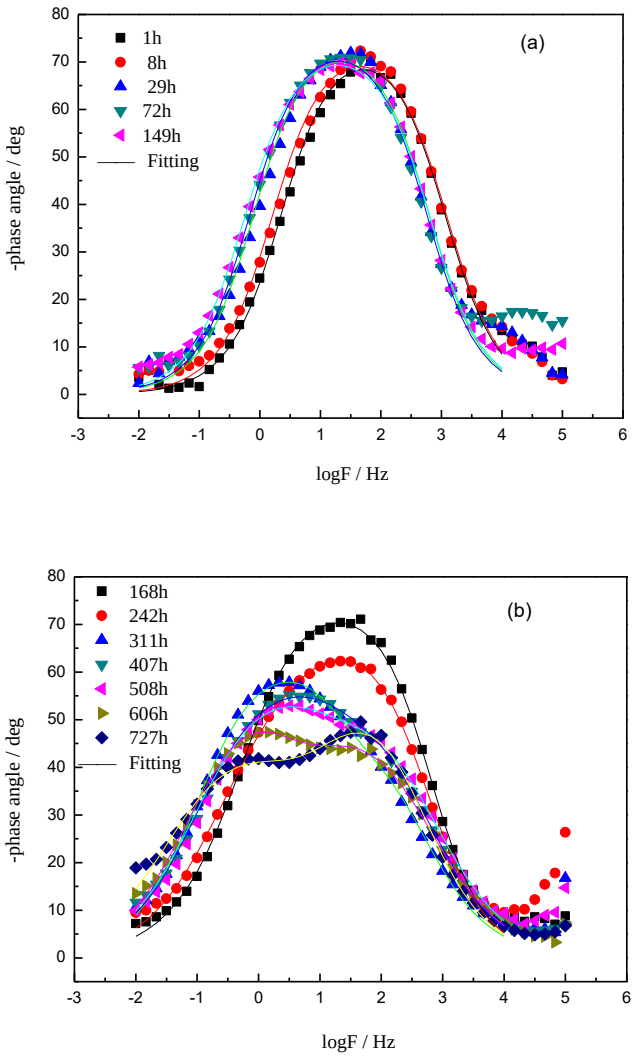

Figure 10. EIS plots of 907A /Ti couple corrosion at different times (a) 0-149 h, (b) 168-720 h.

Table 3. The EIS results for907A /Ti corrosion in seawater from 0h to149h

Time/h	R_S/Ω	CPE1-P/μF	n1	Rct/Ω
0.5	18.77	27.502	0.84695	3548
1	19.46	27.904	0.84700	3820
3.5	19.17	29.355	0.85001	4431
7	18.20	29.513	0.84294	4786
12	18.46	32.611	0.84294	4382
29	19.90	44.333	0.85074	5708
50	23.35	45.114	0.84361	8064
72	25.51	37.367	0.85048	7654
96	26.28	37.001	0.84394	9463
120	27.25	36.566	0.84278	9693
149	27.25	35.793	0.83450	9696

Table 4. The EIS results for 907A /Ti corrosion in seawater from 168 h to720 h

Time/ h	R_S/Ω	CPE1-P/μF	n1	Rm/Ω	CPE2-P/μF	n2	Rct/Ω
168	27.24	34.213	0.84078	10885	630.05	0.77636	2708
198.	28.97	36.828	0.82774	9537	1452.7	0.77636	2779
219	29.72	38.368	0.82234	9166	914.41	0.77636	3687
242	30.99	56.201	0.79137	3976	94.969	0.77636	6683
263	33.17	44.640	0.79702	9750	606.75	0.77636	4277
287	32.79	72.322	0.74200	5479	183.19	0.77636	7094
311	34.5	115.34	0.71643	298.5	42.731	0.77636	8747
336	28.3	170.51	0.65085	873.9	56.025	0.77636	9043
359	32.24	166.54	0.63288	4852	66.736	0.77636	4917
388	33.85	99.618	0.67985	6565	298.69	0.77636	5470
407	37.16	112.31	0.67463	1443	13.012	0.77636	9768
436	36.48	110.21	0.66584	1857	29.944	0.77636	9207
460	34.00	105.89	0.66618	5428	59.257	0.77636	6603
484	35.07	108.82	0.67359	752.5	18.368	0.77636	8974
503	36.48	105.76	0.6665	2548	22.986	0.77636	9125
528	34.21	110.98	0.67769	783.5	48.550	0.77636	7676
533	34.42	110.33	0.67677	761.1	52.901	0.77636	8095
575	36.66	151.63	0.65074	503.1	48.479	0.77636	8190
581	35.72	152.97	0.65181	465.6	56.163	0.77636	8020
599	35.57	145.61	0.65782	451.5	68.969	0.77636	7321
612	38.18	133.53	0.65055	1426	94.500	0.77636	6894
635	37.86	121.94	0.66354	1551	110.68	0.77636	7182
662	40.77	75.837	0.72031	1007	168.49	0.61793	9425
681	39.38	78.500	0.72277	902.2	179.64	0.6359	8286
707	43.26	69.672	0.73145	980.3	215.29	0.58915	9130
727	39.51	75.225	0.73702	806.5	228.00	0.59889	7834

The material with a lower free corrosion potential in the galvanic couple acts as anode and corrodes preferentially [36], but the rate of the galvanic corrosion is determined not only by the

potential differences but also much more by the polarization resistance [37] and so on. Ti is a kind of inert metals [38], a very stable and homogeneous thin oxide film will form on Ti surface even at the room temperature (Reactions (9)-(10)), which film consists of TiO_2 with a thickness of a few nanometers and possesses remarkable corrosion resistance [39-41].

$$Ti + 2e^- \rightarrow Ti^{2+} \quad E^{\theta}(vs.SHE) = -1.63V \qquad (9)$$

$$TiO_2 + 4H^+ + 2e^- \rightarrow Ti^{2+} + 2H_2O \quad E^{\theta}(vs.SHE) = -0.51V \qquad (10)$$

$$Fe + 2e^- \rightarrow Fe^{2+} \quad E^{\theta}(vs.SHE) = -0.45V \qquad (11)$$

$$O_2 + 2H_2O + 4e^- \rightarrow 4OH^- \quad E^{\theta}(vs.SHE) = 0.401V \qquad (12)$$

Based on the standard electrode potential of reactions (10)- (12) which may happen in the corrosive medium, it can be concluded that in 907A/Ti GC, 907A acts as anode while TiO_2 acts as cathode. For the galvanic couple, since the cathode side (TiO_2) has a higher corrosion-resistance comparing with 907A, the tested corrosion information mainly comes from the anode side [42], namely 907A in this study.

During the whole investigated corrosion process of 907A/Ti GC in seawater, CPE1-P also shows the similar variation (Table 3-4) just like that of 907A (Table 1-2), which can also be mainly attributed to the changes of the surface area *S* (Fig.11) and the dielectric constant ε of the corroded interface (formula 1). On the other hand, the CPE1-P value of 907A/Ti GC is somewhat larger than that of 907A, which is caused by both that the corrosion products layer of the former (Fig.11) is more compact than that of the latter (Fig.3) at the same corrosion time, and the electrode area of 907A/Ti GC is two times larger than that of 907A.

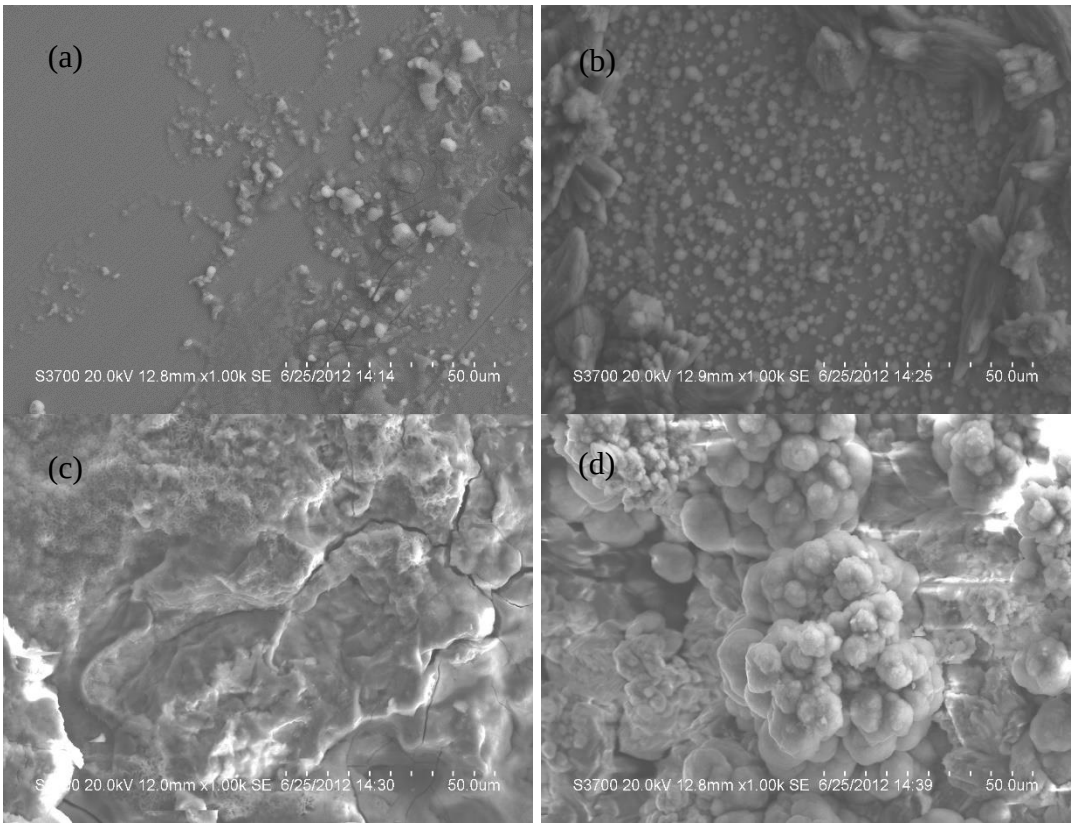

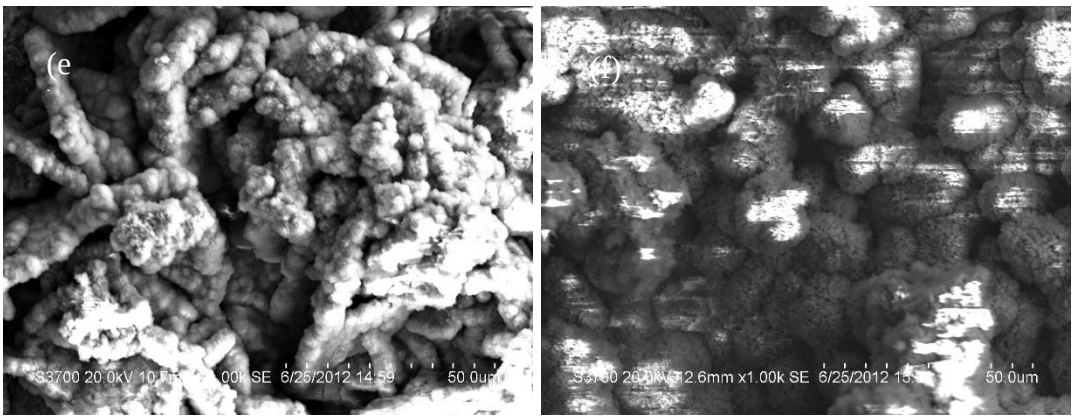

Figure 11. SEM morphologies of 907A in 907A/Ti couple, (a) 0.5 h; (b) 24 h; (c)120 h; (d) 240 h; (e) 480 h; (f) 720 h.

The reciprocal of the sum of *R*ct and *R*m is also used to characterize the corrosion rate [15], which relationship with corrosion time is also plotted in Fig. 2 for comparison. The variation trend of the corrosion rate for 907A/Ti GC is somewhat different to that of 907A. Briefly, (1) the corrosion rate of 907A is always smaller than that of 907A/Ti GC; (2) the demarcation point to distinguish the two corrosion stages for 907A/Ti GC is about 168 h while it is ca. 242h for 907A; (3) in the second corrosion stage, the corrosion rate of 907A/Ti GC increases while that of 907A decreases. The above results indicate that the potential difference between 907A and Ti not only accelerates the corrosion process of the coupled 907A, but also possibly changes its corrosion mechanism.

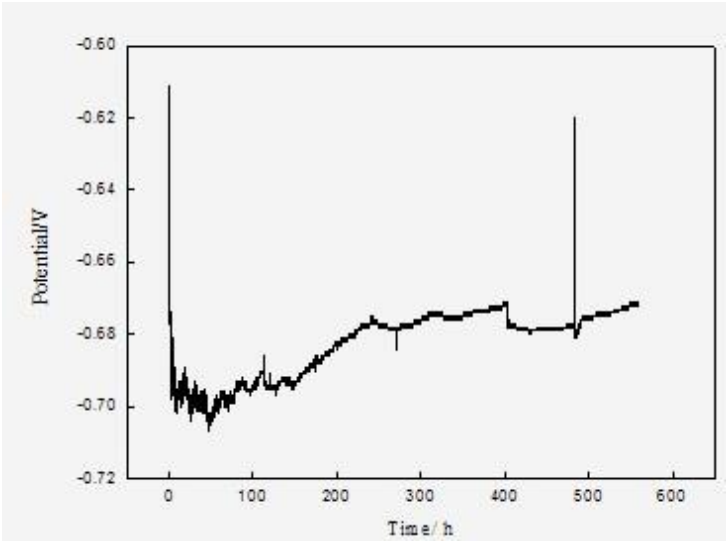

Figure 12. Electrochemical potential noise of 907A/ Ti GC at different times for 580 hours

Fig. 12 is the potential noise (without elimination of dc drift) of 907A/Ti GC corroding in seawater for 580h. For any galvanic couple, which corrosion characteristics mainly reflect that of the anode side [42]. In the case of 907A/Ti GC corrosion, 907A acts mainly as anode and corrodes preferentially. Consequently, the corroding potential variation trend of 907A/Ti GC (Fig.12) is much

similar to that of 907A (Fig.5). Briefly, the ensemble potential noise can also be divided into two stages, i.e., the initial short time of quickly negative drift and the subsequent long time of slowly positive drift, which reason is also similar to that for the potential variation of 907A and has been elucidated above. An obvious difference existed between Fig. 12 and Fig. 5 is that, both the minimum and maximum potentials of 907A/Ti GC are a little negative than those of 907A. For 907A/Ti GC, the measured potential is the mixed potential of 907A and Ti, and the free corrosion potential of Ti is much lower than that of 907A (reactions 7-8), which consequently results in that the measured potential of GC should be lower than that of 907A.

The potential noise shown in Fig. 12 is also analyzed using MEM technique according to its different corrosion stages, the obtained PSD plots and which derived S_E and S_G plots are shown in Figs. 13-14, respectively.

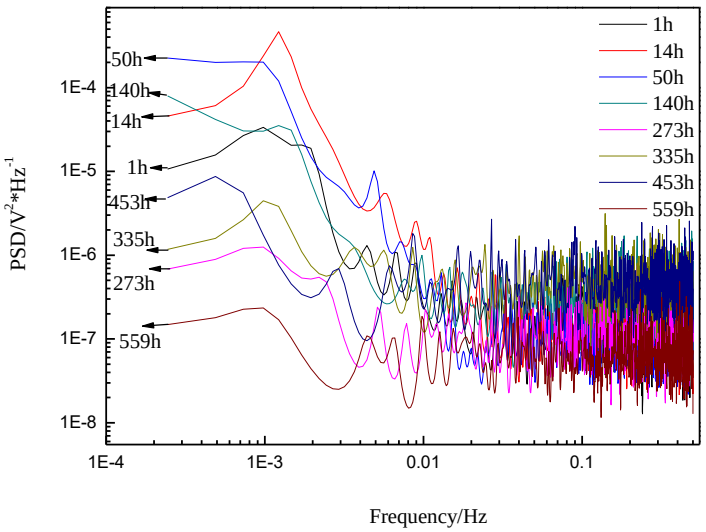

Figure 13. The PSD plots of 907A/ Ti GC in seawater at different corrosion time

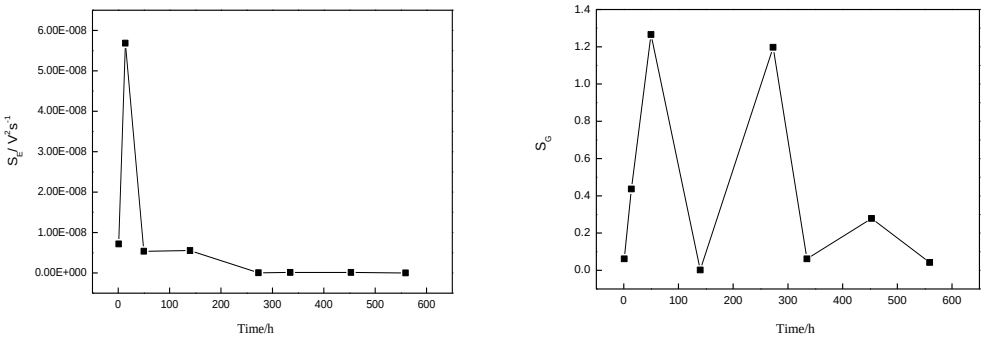

Figure 14. The S_E and S_G value of 907A/ Ti GC corroding in seawater at different time.

The corrosion index S_E in the first corrosion stage of 907A/ Ti GC in seawater (≤ ca. 168h) is much larger than that in its second corrosion stage, and S_G always possesses larger fluctuated values in the whole investigated corrosion time (Fig.14). Meanwhile, when carefully compare Fig.14 with Fig.7, it can be seen that the S_E of 907A/ Ti GC is an order larger than that of 907A, which not only

indicates that the pitting corrosion strength of the former is much higher than that of the latter, but also verifies the result obtained by EIS technique (Fig.4) that the corrosion rate of the former is much larger than the latter. On other words, the potential difference between Ti and 907A markedly accelerates the corrosion process of 907A, which consequently speeds up the diffusion process of the corrosive particles Cl^- and O_2 from the bulk corrosive solution to the corroding surface and presents as the large fluctuated S_G values during the ensemble investigated corrosion time (Fig.14).

The time domain EN data in Fig. 12 are also analyzed using FWT method [30-33], for comparison, the obtained evolution features of the electrochemical active energy (E_a) are also plotted in Fig. 9. From Fig. 9, it can be seen that E_a of 907A/ Ti GC is always larger than that of 907A except their first values. When compared with the results obtained by EIS (Fig. 4) and MEM (Fig. 7 and Fig. 14) analyses, where the corrosion rate of 907A/ Ti GC is larger than that of 907A, it can be concluded that the larger the E_a value, the higher the corrosion rate.

At last, there exists another question, ie. why the first point value of E_a for 907A is larger than that for 907A/ Ti GC (Fig. 9)? The reason may be that, the free potential of Ti is more negative than that of 907A (equation 9-12), therefore, at the beginning of immersion, Ti in the freshly polished 907A/ Ti GC will first proceed to form oxide film TiO_2, which temporarily inhibits the rapid corrosion of 907A.

4. CONCLUSIONS

(1) Both the corrosion process of 907A and 907A /Ti GC can be divided into two stages but with different demarcation points. The first corrosion stage of 907A/Ti GC is shorter than that of 907A. During the whole investigated corrosion time, the corrosion rate of 907A decrease initially quickly and then slowly, whereas the corrosion rate of 907A/Ti GC shows the variation tendency of initially rapid decrease in its first corrosion stage and then slow increase in its second corrosion stage. The potential difference between Ti and 907A markedly accelerates the corrosion process of 907A, and may changes the corrosion mechanism of 907A in 907A/Ti GC.

(2) The electrochemical active energy (E_a) derived from the corrosion noise can be used to correctly characterize the corrosion process of 907A and 907A/Ti GC in seawater; the larger the E_a value, the higher the corrosion rate.

ACKNOWLEDGEMENTS
The authors wish to acknowledge the financial supports from the National Natural Science Foundation of China (Project 21273199, 21403194, 21363018), and the Specialized Research Fund for the Doctoral Program of Higher Education (No. 20130101110047).

References

1. Z. Y. Yang, Ocean University of China, Qingdao, (2009)1.
2. Y. Li, Y. Wang, W. G. Wu, Z. P. Du, X. B. Li, W. Zhang, *J. Harbin Eng. Univ.*, 36(2015)127.

3. R. T. Liu, J. K. Yu, F. C. Jiang, T. F. Zhang, *Mat. For Mech. Eng.*, 26(2002)9.
4. X. M. Liu, Y. Q. Zhang, *J. Iron. And Steel. Res.*, 4(1992)28.
5. X. H. Su, X. D. Kong, K. Wang, Y. H. Hu, *Corros. Sci. Pro. Tech.*, 27(2015)368.
6. Y. Y. Chen, H. J. Tang, L. Wei, *Corros. Sci.*, 47(2005) 1001.
7. F. E. Varela, Y. Kurata, N. Sanada. *Corros. Sci.*, 39(1997) 775.
8. X. Q. Du, Q. S. Yang, Y. Chen, Y. Yang, Z. Zhang, *Trans. Nonferrous Met. Soc.China*, 24(2014)570.
9. N. D. Nam, M. J. Kim, Y. W. Jang, J. G. Kim, *Corros. Sci.*, 52(2010)14.
10. C.F. Dong, K. Xiao, X. G. Li, Y. F. Cheng. *J. Mater. Eng. Perform.* , 20(2011)1631.
11. A. Bakhtari, T. G. Bradley, W. K. Lobb, D. W. Berzins. *Am. J. Orthod.*, 140(2011) 25.
12. X. Q. Huang, Y. Chen, T. W. Fu, Z. Zhang, J. Q. Zhang, *J. Electrochem. Soc.*, 160(2013) 530.
13. Van Der Weijde, D. H., Van Westing, E. P. M., De Wit, J. H. W, *Corros. Sci.*, 36(1994)643.
14. P. Campestrini, E. P. M. Van Westing, J. H. W. de Wit, *Electrochim. Acta*, 46(2001) 2553.
15. D. J. Fang, X. H. Mao, Y. M. Zhang, *Anti-Corros. Methods Mater.*, 56(2009) 226.
16. L. Han, Z. Song, *Corros. Sci.*, 50(2008)1551.
17. F. G. Liu, M. Du, J. Zhang, M. Qiu, *Corros. Sci.*, 51(2009)102.
18. F. Kuang, J. Wang, L. Yan, D. Zhang, *Electrochim. Acta*, 52(2007) 6084.
19. Y. Y. Chen, H. J. Tzeng, L. I. Wei, H.C. Shih, *J. Mater. Sci. Eng. A*, 398(2005)47.
20. Q. Hu, G. Zhang, Y. Qiu, X. Guo, *Corros. Sci.*, 53(2011) 4065.
21. P. C. Searson, J. L. Dawson. *J. Electrochem. Soc.*, 135(1988) 1915.
22. J. Flis, J. L. Dawson, J. Gill, G. C. Wood. *Corros. Sci.*, 32(1991)877.
23. K. Hladky, J. L. Dawson. *Corros. Sci.*, 22(1982) 231.
24. F. Mansfeld, H. Xiao. *J. Electrochem. Soc.*, 140(1993) 2205.
25. Y. Y. Shi, Z. Zhang, J. X. Su, F. H. Cao, J. Q. Zhang. *Electrochim. Acta*, 51(2006) 4977.
26. M. C. Lefebvre, B. E. Conway. *J. Electroanal. Chem.*, 480(2000)46.
27. C. S. Wu, Z. Zhang, F. H. Cao, L. J. Zhang, J. Q. Zhang, C. N. Cao. *Appl. Surf. Sci.*, 253(2007), 3893.
28. C. Cai, Z. Zhang, F. H. Cao, *J. Electroanal. Chem.*, 578(2005)143.
29. F. H. Cao, Z. Zhang, J. X. Su, *Electrochim. Acta*, 51(2006)1359.
30. C. Arya, P.R.W Vassie. *Cem. Concr. Res.*, 25(1995)989.
31. P. Zhang, X. Nie, D.O. Northwood. *Surf. Coat. Technol.*, 203(2009)3271.
32. C. Liu, D. L. Chen, S. Bhole, X. Cao, M. Jahazi. *Mater. Charact.*, 60(2009)370.
33. H. B. Ding, L. H. Hihara. *J. Electrochem. Soc.*, 158(2011)118.
34. A. Aballe, M. Bethencourt, F. J. Botana, M. Marcos, *Electrochim. Acta*, 44(1999)4805.
35. J. A. Wharton, R. J. K. Wood, B. G. Mellor. *Corros. Sci.*, 45(2003)97.
36. G. K. Glass, V. Ashworth. *Corros. Sci.*, 25(1985)971.
37. M. E. EL-Dahshan, A. M. Shams El Din, H .H. Haggag. *Desalination*, 142(2002)161.
38. C. Kuphasuk, Y. Oshida, C. J. Andres, S. T. Hovijitra, M. T. Barco, D. T. Brown. *J. Prosthet. Dent.*, 85(2001)195.
39. E. Blasco-Tamarit, A. Igual-Munoz, J. García Antón, D. M. García-García. *Corros. Sci.*, 59(2009)1095.
40. Q. Lu, J. Alberch, T. Hashimoto, S. J. Garcia-Vergara, H. Habazaki, P. Skeldon, G. E. Thompson. *Corros. Sci.*, 50(2008)548.
41. M. H. O. Kiiniinen, E. T. Lavonius, J. K. Kivilahti. *Dent. Mater.*, 11(1995), 269.
42. J. Z. Ai, X. P. Guo, Z. Y. Chen. *Appl. Surf. Sci*., 253(2006)683.